On Offset-Free Continuous
Model Predictive Current Control
of Permanent Magnet Synchronous Motors

Issa Hammoud [*,**] **Ke Xu** [*] **Sebastian Hentzelt** [*]
Thimo Oehlschlaegel [*] **Ralph Kennel** [**]

*Powertrain Mechatronics, Control Engineering Excellence Cluster,
IAV GmbH, Gifhorn 38518 Germany (e-mail: issa.hammoud@iav.de,
ke.xu@iav.de, sebastian.hentzelt@iav.de, thimo.oehlschlaegel@iav.de)*
** *Institute for Electrical Drive Systems and Power Electronics,
Technical University of Munich (TUM), Munich, Germany. (e-mail:
issa.hammoud@tum.de, ralph.kennel@tum.de)*

Abstract: In this work, an offset-free continuous control set model predictive current control (CCS-MPCC) strategy for synchronous machines based on a slack formulation of the Primal-Dual Interior-Point method is proposed. A horizon of two steps is achieved within 100 µs sampling period. To account for robustness against model mismatch and uncertainty, an incremental formulation of the MPC problem is used to ensure zero steady-state tracking error. The proposed controller is compared with the state of the art Field Oriented Control with PI controllers (FOC-PI), with the Deadbeat Model Predictive Current Control (DB-MPCC), and with the latter controller combined with discrete integrators in the feedback loop (DB-MPCC-I). Experimental results on a 0.5 kW PMSM prove that the proposed CCS-MPCC has outperformed the state of the art control techniques typically used to control electrical machines.

Keywords: continuous control set model predictive control, permanent magnet synchronous motors, online optimization, electrical drives.

1. INTRODUCTION

Due to their diverse beneficial features such as the reliable and compact design as well as the high efficiency and power density, permanent magnet synchronous motors (PMSMs) have recently gained an ascending interest, especially in high dynamic applications such as the traction system in the automotive field (Huynh and Hsieh (2018)).

Different control methods have been implemented to control synchronous motors fed by voltage source inverter (VSI), such as field oriented control (FOC) with cascaded PI controllers (Schröder (2009)), direct torque control DTC (Lascu et al. (2004)), and more recently finite control set model predictive control (FCS-MPC) (Hammoud et al. (2019)) as well as continuous control set model predictive control (CCS-MPC) (Hanke et al. (2019)).

The state of the art FOC-PI suffers from non-optimal transient response accompanied by overshooting, and it also has a poor response against load variation when compared to optimization-based controllers. Furthermore, it needs to be combined with anti-windup schemes and feed-forward decoupling. Whereas DTC is characterized by its fast dynamical response and its low computational demand, it suffers from high current distortions and tracking ripples due to the absence of a modulator. Thus, it operates at an unfavorable variable switching frequency lower than the sampling frequency, which results in acoustic noise.

Since the beginning of the current millennium, model predictive control (MPC) started to gain a genuine interest in the field of electrical drive systems and power electronics (Kennel et al. (2001)). Principally, this is because it easily allows the handling of inputs and states constraints. Moreover, it allows the design of a specific trade-off between tracking ripple and switching events (switching losses), which is considered as an additional degree of freedom in the controller design even though this requires longer prediction horizons.

Based on prior knowledge of the mathematical model describing the plant under control, MPC aims to solve an optimal control problem (OCP) over a receding horizon. The control objective is expressed as a cost functional, where the minimum corresponds to the desired system behavior. In the case of the PMSM, discretizing the cost functional with respect to time and considering the finite set of control actions being offered by the inverter, the OCP can be transformed into a mixed integer problem. A possible solution to solve this problem is a combinatorial approach in which the solution is being found from a finite set of possible candidates (in the case of a 2-level VSI: the eight possible output voltage vectors of the inverter). Hence, is called finite control set model predictive control (FCS-MPC). Otherwise, it can be solved through solving optimization problems on continuous sets to calculate the optimal voltage vector (VV) in which so-called continuous control set model predictive control (CCS-MPC), and realize it using a modulator.

In electrical drives, CCS-MPC achieves a much better steady-state performance in terms of tracking ripples when compared to FCS-MPC, albeit this better performance comes at the expense of having more switching events at each switching period (i.e. more losses). In Comparison with the linear FOC and DTC, CCS-MPC combines the best features of them both in terms of fast transient behavior and minimal steady-state tracking ripples.

In particular, CCS-MPC is of high interest in applications where the model of the plant is nonlinear or is exposed to nonlinear input and/or output constraints. These reasons make CCS-MPC a very convenient and promising control approach for PMSM drive systems.

Generally, the PMSM drive system is subject to uncertainties (i.e. parameters mismatch, especially in the inductance) as well as external disturbances. This uncertainty will lead to a sub-optimal control performance (i.e. tracking bias or higher ripples on the tracked reference trajectories, overshooting or slower dynamical response in transients, and in severe cases it may lead to instability).

Solving the optimization problem online within the submillisecond sampling periods available in electrical drive applications is challenging. Consequently, the deadbeat function with the prediction model is commonly used to analytically compute the continuous VV which will drive the states to their desired references. However, model mismatch and unmodeled dynamics severely impact the performance of this method.

In this paper, a robust and offset-free continuous set model predictive current controller is designed based on the incremental model of the plant. The decision variables of the OCP are the control input increments, and the optimization problem is solved online for a horizon of two. The proposed controller is experimentally validated and compared to FOC-PI, DB-MPCC, and the DB-MPCC-I.

The rest of the paper is structured as follows: the mathematical modelling of a 2-level inverter and a permanent magnet synchronous machine are introduced in Section 2. The state of the art FOC is presented in Section 3, the DB-MPCC and DB-MPCC-I are presented in Section 4 and Section 5, respectively. The proposed CCS-MPCC controller design is then presented in Section 6. The experimental setup and the test bench components are described in Section 7. In Section 8, the experimental results of the proposed controller are presented and compared with those of the other three controllers mentioned in the paper. Finally, the paper is concluded in Section 9.

2. MATHEMATICAL MODELLING

The mathematical models describing the plant under control are established in the following:

2.1 Modelling of a 2-level VSI

The most commonly used DC to AC inverter especially in low-to-medium power applications is the two-level inverter, which consists of six switches with parallel free wheeling diodes. The input side consists of the DC link which has a specific DC input voltage that will be modulated to form the output three-phase AC voltage to drive
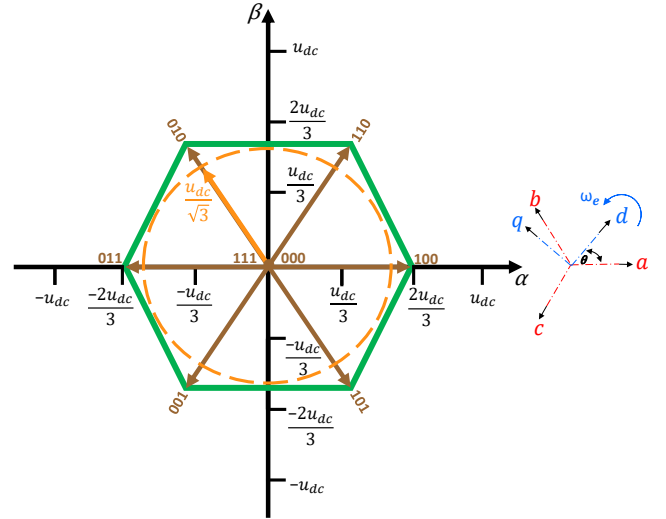
Fig. 1. Voltage vectors of a 2-level voltage source inverter

the electric machine. The gates of the upper and lower switches of each leg of the inverter must have complementary driving signals. Their transition states are shifted with appropriate dead times to avoid short circuit on the input side (Hackl (2017)).

The instantaneous phase-to-phase voltage u_f^{ptp} on the output of the inverter is expressed in terms of DC link voltage $u_{dc}(t)$ and the switching states vector $\boldsymbol{S}^{abc} = \begin{pmatrix} S^a \\ S^b \\ S^c \end{pmatrix} \in$

$$\mathbb{S} := \left\{ \begin{pmatrix} 1 \\ 1 \\ 1 \end{pmatrix}, \begin{pmatrix} 1 \\ 0 \\ 0 \end{pmatrix}, \begin{pmatrix} 1 \\ 1 \\ 0 \end{pmatrix}, \begin{pmatrix} 0 \\ 1 \\ 0 \end{pmatrix}, \begin{pmatrix} 0 \\ 1 \\ 1 \end{pmatrix}, \begin{pmatrix} 0 \\ 0 \\ 1 \end{pmatrix}, \begin{pmatrix} 1 \\ 0 \\ 1 \end{pmatrix}, \begin{pmatrix} 0 \\ 0 \\ 0 \end{pmatrix} \right\}$$

as

$$\boldsymbol{u}_f^{ptp}(t) = [u_f^{ab}(t), u_f^{bc}(t), u_f^{ca}(t)]^T = u_{dc}(t)\boldsymbol{T}^{ptp}\boldsymbol{S}^{abc}(t), \tag{1}$$

where $\boldsymbol{T}^{ptp}$ is the coefficient matrix and is defined as

$$\boldsymbol{T}^{ptp} = [1, -1, 0; 0, 1, -1; -1, 0, 1]. \tag{2}$$

The three phase stator voltages are then defined as

$$\boldsymbol{u}_f^{abc}(t) = [u_f^a(t), u_f^b(t), u_f^c(t)]^T = \frac{u_{dc}(t)}{3}\boldsymbol{T}^{abc}\boldsymbol{S}^{abc}(t), \tag{3}$$

where the coefficient matrix $\boldsymbol{T}^{abc}$ is defined as

$$\boldsymbol{T}^{abc} = [2, -1, -1; -1, 2, -1; -1, -1, 2]. \tag{4}$$

and $\boldsymbol{u}_f^{(.)}(t) \in \{0, \frac{u_{dc}(t)}{3}, \frac{2u_{dc}(t)}{3}, \frac{-u_{dc}(t)}{3}, \frac{-2u_{dc}(t)}{3}\}$, for $(.) \in \{a, b, c\}$.

From now on, the time-dependent notation will be dropped for simplicity. Using Clarke and Park transformations one after another, the inverter voltages in the stationary α-β and the rotating dq reference frames are expressed as

$$\begin{bmatrix} u_f^\alpha \\ u_f^\beta \end{bmatrix} = \frac{2}{3} \begin{bmatrix} 1 & -\frac{1}{2} & -\frac{1}{2} \\ 0 & \frac{\sqrt{3}}{2} & -\frac{\sqrt{3}}{2} \end{bmatrix} \begin{bmatrix} u_f^a \\ u_f^b \\ u_f^c \end{bmatrix}, \tag{5}$$

and

$$\begin{bmatrix} u_f^d \\ u_f^q \end{bmatrix} = \begin{bmatrix} cos(\theta) & sin(\theta) \\ -sin(\theta) & cos(\theta) \end{bmatrix} \begin{bmatrix} u_f^\alpha \\ u_f^\beta \end{bmatrix}, \tag{6}$$

respectively, where θ is the rotation angle. The output voltage vectors of a 2-level VSI are shown in Fig. 1.

2.2 Modelling of a PMSM

In this subsection, the mathematical model of a three-phase interior permanent magnet synchronous motor (IPMSM) is considered ($L_d \neq L_q$). In the dq reference frame, the model is expressed as

$$u_d = R_s i_d + L_d \frac{di_d}{dt} - \omega_e L_q i_q, \tag{7a}$$

$$u_q = R_s i_q + L_q \frac{di_q}{dt} + \omega_e L_d i_d + \omega_e \Psi_{pm}, \tag{7b}$$

where u_d and u_q are the d-axis and q-axis phase voltages (in V), i_d and i_q are the stator currents in the dq reference frame (in A), L_d and L_q are the stator inductances (in H), R_s is the stator resistance (in Ω), Ψ_{pm} is the permanent-magnet flux linkage (in Wb), and ω_e is the electrical angle (in rad s^{-1}).

The states, inputs, and outputs vectors are defined as $\boldsymbol{x}$, $\boldsymbol{u}$, and $\boldsymbol{y}$, respectively with $\boldsymbol{x} \in \mathbb{R}^{N_x}$, $\boldsymbol{u} \in \mathbb{R}^{N_u}$, and $\boldsymbol{y} \in \mathbb{R}^{N_y}$, where N_x, N_u, and N_y are the number of states, inputs, and outputs. By using explicit Euler discretization method, the current prediction model is obtained as

$$\begin{bmatrix} i_{d,k+1} \\ i_{q,k+1} \end{bmatrix} = \begin{bmatrix} i_{d,k} \\ i_{q,k} \end{bmatrix} + T_s \begin{bmatrix} \frac{-R_s i_d}{L_d} + \frac{L_q \omega_e i_q}{L_d} + \frac{u_d}{L_d} \\ \frac{-R_s i_q}{L_q} - \frac{L_d \omega_e i_d}{L_q} + \frac{u_q}{L_q} - \frac{\psi_{pm} \omega_e}{L_q} \end{bmatrix}, \tag{8}$$

with k as the time step index and T_s as the sampling time.

3. FIELD ORIENTED CURRENT CONTROL BASED ON PI CONTROLLERS

The state of the art field oriented control is based on instantaneously decoupling the direct and quadrature components of the electrical machine's current, which allows separate control of the torque and flux of the electric engine. Normally, it is combined with feedforward decoupling to be able to control both currents on the dq reference frame independently (Schröder (2009)). In this paper, it is briefly introduced and its performance is tested and compared with the DB-MPCC, the DB-MPCC-I, and the proposed CCS-MPCC. The schematic diagram of the classical FOC control scheme of a PMSM is shown in Fig. 2.(a).

4. DEADBEAT MODEL PREDICTIVE CURRENT CONTROL

In general, continuous MPC is computationally very demanding as the execution time to solve the optimization problem increases significantly with the length of the prediction horizon as well as the number of the decision variables. A common way to overcome the high computational demand within the short available sampling times in the field of electrical machines control is to substitute the deadbeat function of the current prediction model (8) by assuming that the ultimate tracking objective is met

$$\begin{bmatrix} i_{d,k+1} \\ i_{q,k+1} \end{bmatrix} = \begin{bmatrix} i_{d,k+1}^{ref} \\ i_{q,k+1}^{ref} \end{bmatrix}, \tag{9}$$

where the reference predicted current at $k+1$ can be computed using linear extrapolation. Hence, the reference control input can be calculated analytically. By subtracting the current predictions between two consecutive time
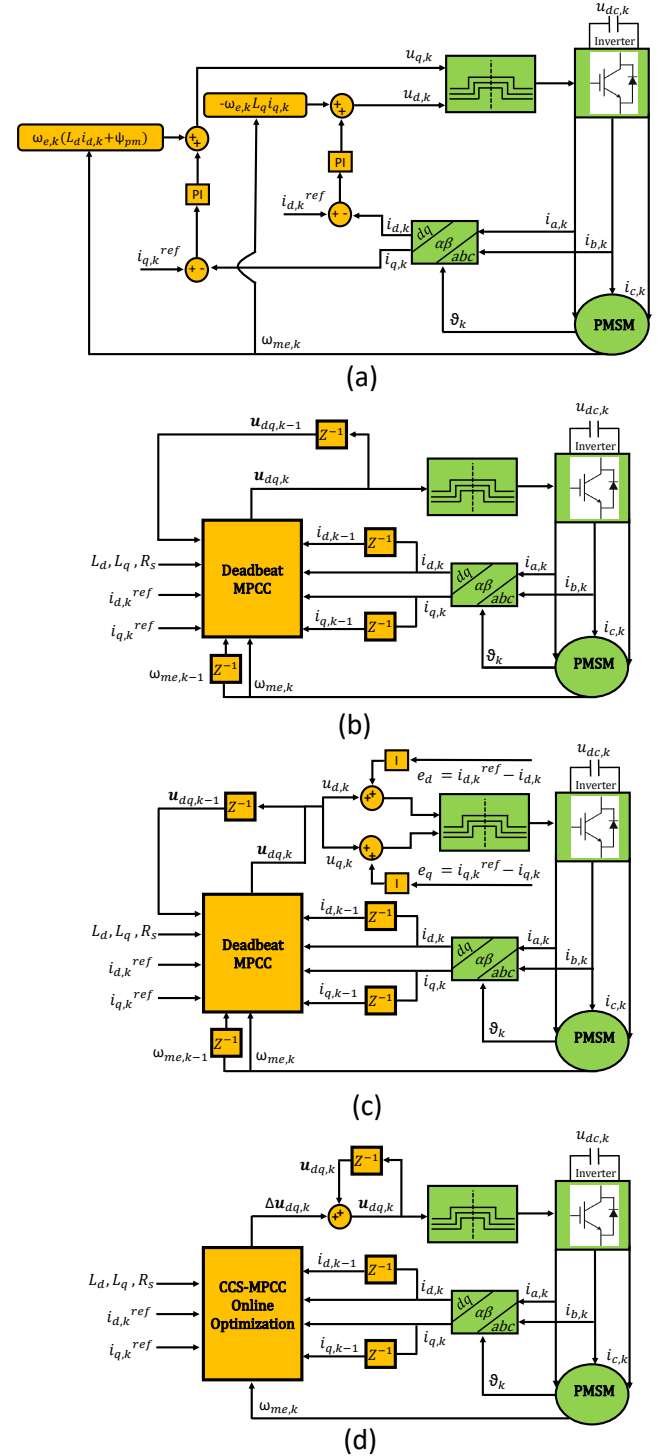
Fig. 2. Control schemes: (a) FOC with PI controllers and feedforward decoupling, (b) Deadbeat model predictive current control (DB-MPCC), (c) Deadbeat model predictive current control with integrators in the feedback loop (DB-MPCC-I), (d) Proposed CCS-MPCC based on input increments

instants (e.g. $\boldsymbol{i}_{dq,k+1} - \boldsymbol{i}_{dq,k}$, with $\boldsymbol{i}_{dq,k} := [i_{d,k} \quad i_{q,k}]^T$), and rearranging the equation in terms of the current at the latter time instant $k+1$, the flux linkage term disappears from the prediction model, and hence, eliminating one source of possible model mismatch impact on the predictions accuracy as can be seen from the analytical

expression of the control inputs (i.e. voltages to be applied to the machine)(Hammoud et al. (2019))

$$u_{d,k} = u_{d,k-1} + \frac{L_d}{T_s}(i_{d,k+1}^{ref} + i_{d,k-1})$$
$$- L_q(\omega_{e,k}i_{q,k} - \omega_{e,k-1}i_{q,k-1})$$
$$- \frac{2L_d}{T_s}i_{d,k} + R_s(i_{d,k} - i_{d,k-1}), \quad (10a)$$

$$u_{q,k} = u_{q,k-1} + \frac{L_q}{T_s}(i_{q,k+1}^{ref} + i_{q,k-1})$$
$$+ L_d(\omega_{e,k}i_{d,k} - \omega_{e,k-1}i_{d,k-1})$$
$$- \frac{2L_q}{T_s}i_{q,k} + R_s(i_{q,k} - i_{q,k-1}). \quad (10b)$$

Even though this control method is characterized by its very fast dynamic response and simplicity (i.e. very short demanded computational time), it is obvious from equation (10) that the control laws will be highly affected by any disturbance, model mismatch or uncertainty. Inductance mismatch (Young et al. (2016)), as well as the inverter nonlinearity (Wiedemann and Kennel (2018)) in case not estimated/compensated accurately, they will negatively affect the accuracy of the predictions. Consequently, these lead to unwanted effects such as higher ripples, acoustic noise, and non-zero steady-state tracking performance. This will be very clear in terms of tracking offsets and higher ripple (i.e. inaccurate predictions) in the experimental results section, where the machine's parameters which are fed to the controller are assumed to be constant (i.e. without online observers or offline inductance variation maps), and without inverter nonlinearity compensation mechanism. The schematic diagram of the DB-MPCC scheme is illustrated in Fig. 2.(b).

5. DEADBEAT MODEL PREDICTIVE CURRENT CONTROL WITH AN INTEGRATOR IN THE FEEDBACK LOOP

One simple way to enhance the steady-state performance of the DB-MPCC is to include a discrete-time integrator in the feedback loop. Hence, the control input commands, which will be applied to the machine, are the control laws shown in (10), added to the discrete error integration signals

$$u_{d,k+1}^{err} = K_i \sum_{i=0}^{k} i_{d,i}^{meas} - i_{d,i}^{ref}, \quad (11a)$$

$$u_{q,k+1}^{err} = K_i \sum_{i=0}^{k} i_{q,i}^{meas} - i_{q,i}^{ref}. \quad (11b)$$

This ensures a zero steady-state tracking error. However, it comes at the expense of worsening the tracking performance at load variations as will be seen from the experimental results. The schematic diagram of the DB-MPCC-I scheme is illustrated in Fig. 2.(c).

6. CONTINUOUS CONTROL SET MODEL PREDICTIVE CURRENT CONTROL (CCS-MPCC) BASED ON ΔU FORMULATION

Considering the discrete time linear system of the electrical machine

$$x_k = Ax_{k-1} + Bu_{k-1} + d_{k-1}, \quad (12)$$

which is obtained by discretizing the model (7a and 7b) using explicit Euler discretization method. For one step ahead

$$x_{k+1} = Ax_k + Bu_k + d_k, \quad (13)$$

with

$$A = \begin{bmatrix} 1 - \frac{T_s R_s}{L_d} & \frac{L_q}{L_d}T_s\omega_{e,k} \\ -\frac{L_d}{L_q}T_s\omega_{e,k} & 1 - \frac{T_s R_s}{L_q} \end{bmatrix}, B = \begin{bmatrix} \frac{T_s}{L_d} & 0 \\ 0 & \frac{T_s}{L_q} \end{bmatrix},$$

$$x_k = \begin{bmatrix} i_{d,k} \\ i_{q,k} \end{bmatrix}, u_k = \begin{bmatrix} u_{d,k} \\ u_{q,k} \end{bmatrix}, d_k = \begin{bmatrix} 0 \\ -\frac{T_s\omega_{e,k}\psi_{pm,k}}{L_q} \end{bmatrix}.$$

Assuming ω_e and ψ_{pm} to be constant between two consecutive time instants, such as: $\omega_{e,k} \approx \omega_{e,k-1}$ and $\psi_{pm,k} \approx \psi_{pm,k-1}$, an incremental model is defined as

$$\Delta x_{k+1} = x_{k+1} - x_k, \quad (14a)$$
$$= A\Delta x_k + B\Delta u_k, \quad (14b)$$
$$\Delta u_k = u_k - u_{k-1}. \quad (14c)$$

Rearranging (14) in terms of x_{k+1}, the states prediction model is obtained as

$$x_{k+1} = x_k + A\Delta x_k + B\Delta u_k, \quad (15)$$

where it is clear that the non-zero constant disturbance term d_k disappeared in (15). Considering Δu_k as decision variables vector, the control input that is being given to the plant at each time instant k is expressed from (14c) as

$$u_k = \Delta u_k + u_{k-1}. \quad (16)$$

The output vector is identical to the states vector and all states are measured. The states increment vector is defined in terms of the current and previously measured states (i.e. x_k and x_{k-1}), the previous known/measured control inputs (i.e. u_{k-1}), and the model parameters. Hence, there is no need for states observer. The formulation of the OCP in terms of the input increments as decision variables benefits the performance of the current control of the electrical machine by its embedded error integration functionality (i.e. guarantees a zero steady-state tracking error) (Sharma (2019)). Also, the elimination of the flux linkage term in the prediction model, which would affect the prediction accuracy in case of mismatch.

The standard cost function that penalizes the deviation of the machine's current from its reference is used in this paper, and it is formulated as

$$J(\Delta U) = \frac{1}{2}\sum_{i=0}^{N-1}(y_{k+1+i|k} - r_k)^T Q(y_{k+1+i|k} - r_k)$$
$$+ \Delta u_{k+i|k}^T R\Delta u_{k+i|k}, \quad (17)$$

where $Q = Q^T \geq 0$ and $R = R^T > 0$ are weighting matricies with corresponding dimensions, $y_{k+1+i|k} := [i_{d,k+1+i} \quad i_{q,k+1+i}]^T$ is the predicted current vector at time instant $k + 1 + i$ using the knowns at time instant k (i.e. previously calculated or measured control inputs as well as actual and previously measured outputs/states), $r_k := [i_{d,k}^* \quad i_{q,k}^*]^T$ is the reference output vector, $\Delta u_{k+i|k} := [u_{k+i|k} - u_{k+i-1|k}]^T$ is the input increment vector, $\Delta U := (\Delta u_k, ..., \Delta u_{k+N-1})$ are the input increments along the horizon as decision variables, and N is the prediction horizon.

The constrained optimization problem considered in this work for a horizon of two is stated as

$$\min_{\Delta \boldsymbol{u}_k, \Delta \boldsymbol{u}_{k+1}} \quad J(\Delta \boldsymbol{u}_k, \Delta \boldsymbol{u}_{k+1}) \tag{18a}$$

$$\text{s.t.} \quad \boldsymbol{x}_{k+1} = \boldsymbol{x}_k + \boldsymbol{A}\Delta \boldsymbol{x}_k + \boldsymbol{B}\Delta \boldsymbol{u}_k \tag{18b}$$

$$\boldsymbol{x}_{k+2} = \boldsymbol{x}_{k+1} + \boldsymbol{A}\Delta \boldsymbol{x}_{k+1} + \boldsymbol{B}\Delta \boldsymbol{u}_{k+1} \tag{18c}$$

$$\boldsymbol{x}_{min} \le \boldsymbol{x}_{k+1} \le \boldsymbol{x}_{max} \tag{18d}$$

$$\boldsymbol{x}_{min} \le \boldsymbol{x}_{k+2} \le \boldsymbol{x}_{max} \tag{18e}$$

$$\Delta \boldsymbol{u}_{min} \le \Delta \boldsymbol{u}_k \le \Delta \boldsymbol{u}_{max} \tag{18f}$$

$$\Delta \boldsymbol{u}_{min} \le \Delta \boldsymbol{u}_{k+1} \le \Delta \boldsymbol{u}_{max} \tag{18g}$$

$$u_{d,k+j}^2 + u_{q,k+j}^2 \le (\frac{u_{dc}}{\sqrt{3}})^2 \forall j \in \{0,1\} \tag{18h}$$

$$i_{d,k+j+1}^2 + i_{q,k+j+1}^2 \le I_{max}^2 \forall j \in \{0,1\} \tag{18i}$$

The maximum and minimum bounds of the voltage vector are constrained to within the circle inscribed in the voltage hexagon of the 2-level VSI, where the amplitude of the current vector is constrained to be within a specific maximum current value I_{max}.

For the real-time implementation of the proposed controller, the optimization problem (18) is solved online using a slack formulation of the Primal-Dual Interior-Point (IP) method. The IP solver is explained in the following subsection. The experimental results shown in a following section proved that the proposed controller presented here has outperformed the state of the art FOC and the well-known conventional MPCC based on the deadbeat function (with and without integrator) in both transients and steady state. The schematic diagram of the proposed CCS-MPCC is presented in Fig. 2.(d).

6.1 Interior Point Solver

In this section, a detailed pseudo code of the implemented Interior-Point solver is presented. The solver is based on a slack formulation of the Primal-Dual Interior-Point method (Diehl (2016)). The goal is to help the other interested readers to easily implement the algorithm. Therefore, the dimension of the zeros matrices O and the identity matrices I is given explicitly. The solver depends on the solution of linear system of equations, which makes it easier to be deployed in different hardware systems.

Due to the limited computation time in electrical drive applications, only an approximate solution of the optimization problem is sufficient. In order to be fast, the standard Primal-Dual Interior-Point method is modified in this paper as follows: Firstly, the barrier parameter τ is fixed. This is the same as proposed in the paper (Wang and Boyd (2010)). Secondly, the maximum iteration number of the IP algorithm is set to be 4.

The algorithm takes the initial guess of the decision variables vector $\boldsymbol{\xi}_k = [\Delta \boldsymbol{u}_k; \Delta \boldsymbol{u}_{k+1}]$ as an input. It repeatedly formulate the KKT system based on the current value of the primal variable $\boldsymbol{\xi}_k$, the dual variables $\boldsymbol{\mu}_k$, $\boldsymbol{\lambda}_k$ and the slack variable $\boldsymbol{s}_k$. Note, that the .* operation in r_T means elementwise multiplication. The KKT system is then solved. After the Newton direction is computed, a line search is performed to ensure a reasonable reduction within the step. In order to keep the computational cost low, the maximum iteration number for the line search is selected to be 12. The scaling factor α is reduced in each line search iteration until all elements in the dual variable for inequality constraints or in the slack variable
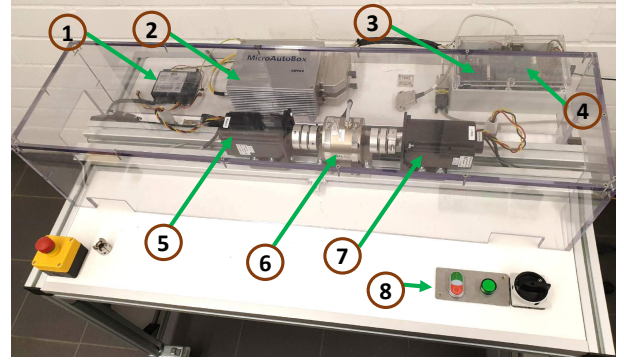
Fig. 3. Test bench components: (1): OttBox controller, (2) dSpace MicroAutoBox II 1513/1514, (3) 2-level VSI from TEXAS Instruments, (4) currents and voltages mesurements board, (5) load machine, (6) torque sensor, (7) main machine, (8) main power switch

are positive. After α is computed, a scaled Newton update is performed, and $\boldsymbol{\xi}_k$ is returned as the output of the algorithm.

The algorithm is illustrated in Algorithm 1, for which:

$$\min_{\boldsymbol{\xi}} \quad J(\boldsymbol{\xi}) (18a)$$

$$\text{s.t.} \quad g(\boldsymbol{\xi}) = 0, (18b, 18c)$$
$$h(\boldsymbol{\xi}) \le 0 (18d - 18i)$$

n_v: the number of decision variables.
n_i: the number of inequality constraints.
n_e: the number of equality constraints.
H: the hessian of the lagrangian.
$\mathcal{L}$: the lagrangian, and is defined as:

$$\mathcal{L} = J(\boldsymbol{\xi}) + \boldsymbol{\lambda}^T g(\boldsymbol{\xi}) + \boldsymbol{\mu}^T h(\boldsymbol{\xi}).$$

7. EXPERIMENTAL SETUP

The test bench where the proposed CCS-MPCC, the DB-MPCC with and without integrator in the feedback loop, and the state of the art FOC based on PI controllers have been tested is shown in Fig 3. The test bench consists of two identical 500 W PMSMs. Both machines are mechanically coupled via a torque sensor (the sensor is not used in this work). The machine on the left side is acting as a load machine and is controlling the rotor mechanical speed via OttBox (commercially available controller). All current control schemes are deployed into a dSpace MicroAutoBox II 1514/1513 real-time platform with MATLAB/Simulink and Control Desk 5.6 interface. The used sampling as well as switching frequency is 10 kHz, and the dead-time for the switches is set to 0.5 μs.

Algorithm 1 Primal-Dual Interior-Point solver

Input: $\boldsymbol{\xi}_k$

Set $\tau = 0.5$, $\boldsymbol{\mu}_k = \boldsymbol{I}(n_i, 1)$, $\boldsymbol{s}_k = \boldsymbol{I}(n_i, 1)$, $\boldsymbol{\lambda}_k = \boldsymbol{I}(n_e, 1)$

for $i = 1$ *to Maximum Number of Iterations* **do**

   ▷ Evaluate $\boldsymbol{H}$, $\boldsymbol{g}$, $\boldsymbol{h}$, $\nabla\boldsymbol{g}$, $\nabla\boldsymbol{h}$, $\nabla\boldsymbol{J}$, and $\boldsymbol{r}_T$

   ▷ Formulate the linear system of equations (KKT)

$$\begin{bmatrix} \boldsymbol{H}(\boldsymbol{\xi}_k, \boldsymbol{\mu}_k, \boldsymbol{\lambda}_k) & \nabla\boldsymbol{g}(\boldsymbol{\xi}_k) & \nabla\boldsymbol{h}(\boldsymbol{\xi}_k) & \boldsymbol{O}(n_v, n_i) \\ \nabla\boldsymbol{g}(\boldsymbol{\xi}_k)^T & \boldsymbol{O}(n_e, n_e) & \boldsymbol{O}(n_e, n_i) & \boldsymbol{O}(n_e, n_i) \\ \nabla\boldsymbol{h}(\boldsymbol{\xi}_k)^T & \boldsymbol{O}(n_i, n_e) & \boldsymbol{O}(n_i, n_i) & \boldsymbol{I}(n_i, n_i) \\ \boldsymbol{O}(n_i, n_v) & \boldsymbol{O}(n_i, n_e) & diag(\boldsymbol{s}) & diag(\boldsymbol{\mu}) \end{bmatrix} \begin{bmatrix} \Delta\boldsymbol{\xi} \\ \Delta\boldsymbol{\lambda} \\ \Delta\boldsymbol{\mu} \\ \Delta\boldsymbol{s} \end{bmatrix}$$

$= -\boldsymbol{r}_T$,with

$$\boldsymbol{r}_T = \begin{bmatrix} \nabla\boldsymbol{J}(\boldsymbol{\xi}_k) + \nabla\boldsymbol{g}(\boldsymbol{\xi}_k)\boldsymbol{\lambda}_k + \nabla\boldsymbol{h}(\boldsymbol{\xi}_k)\boldsymbol{\mu}_k \\ \boldsymbol{g}(\boldsymbol{\xi}_k) \\ \boldsymbol{h}(\boldsymbol{\xi}_k) + \boldsymbol{s}_k \\ \boldsymbol{v}_k .* \boldsymbol{s}_k - \tau \end{bmatrix}$$

   ▷ Compute the Newton direction $[\Delta\boldsymbol{\xi} \ \Delta\boldsymbol{\lambda} \ \Delta\boldsymbol{\mu} \ \Delta\boldsymbol{s}]^T$ by solving the linear KKT equation system.

   ▷ Perform line search and compute an $\alpha \in]0, 1]$ to ensure progress.

   ▷ Initialize $\alpha = 1$, and decrease factor $k_{ls} = 0.9$

   for $j = 1$ *to Maximum Line Search Iterations* **do**

      ▷ Compute trial step based on the following equation

$$\boldsymbol{\mu}_t = \boldsymbol{\mu}_k + \alpha\Delta\boldsymbol{\mu},$$
$$\boldsymbol{s}_t = \boldsymbol{s}_k + \alpha\Delta\boldsymbol{s};$$

      if *All element in* $\boldsymbol{\mu}_t > 0$ *&& all element in* $\boldsymbol{s}_t > 0$ **then**

         break; (Scaling factor α is found)

      end

      ▷ Decrease α:

$$\alpha = \alpha k_{ls}$$

   end

   ▷ Take Newton step:

$$\boldsymbol{\xi}_k = \boldsymbol{\xi}_k + \alpha\Delta\boldsymbol{\xi},$$
$$\boldsymbol{\lambda}_k = \boldsymbol{\lambda}_k + \alpha\Delta\boldsymbol{\lambda},$$
$$\boldsymbol{\mu}_k = \boldsymbol{\mu}_k + \alpha\Delta\boldsymbol{\mu},$$
$$\boldsymbol{s}_k = \boldsymbol{s}_k + \alpha\Delta\boldsymbol{s};$$

   if $\|\boldsymbol{r}_T\|_2 \leq threshold$ **then**

      break; (Approximate solution is found)

   end

end

Output: $\boldsymbol{\xi}_k$

Table 1. Parameters of the IPMSM

Name	Nomenclature	Value
DC-link voltage	u_{dc}	48 V
Maximum Current	I_{max}	10 A
Stator resistance	R_s	0.0385 Ω
D-axis inductance	L_d	50 μH
Q-axis inductance	L_q	65 μH
Sampling frequency	f_s	10 kHz
Flux Linkage	Ψ_{pm}	0.02 Vs/rad

8. EXPERIMENTAL RESULTS

In this section, the performance of the proposed CCS-MPCC is firstly presented through an ascending and
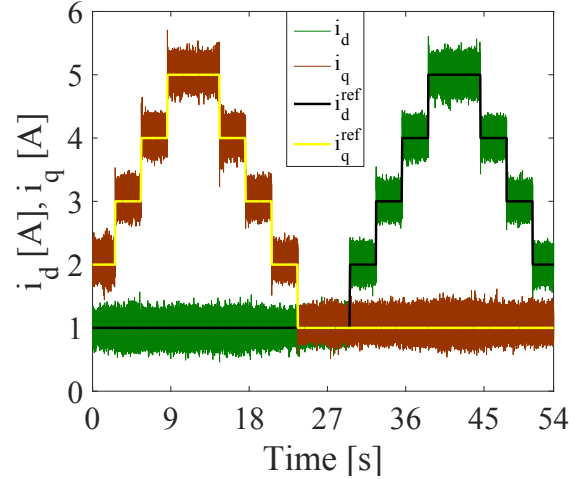
Fig. 4. Current tracking with the proposed CCS-MPCC at 500 RPM
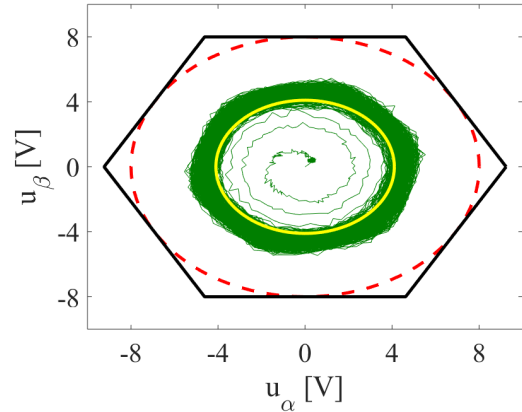
Fig. 5. Voltage trajectory (green) that produced the currents shown in Fig. 4 (the red dashed circle radius = 8V), the yellow circle has a radius of 4V to be linked with the next scenario shown in Fig. 6

descending reference current profile being applied to the main PMSM, while applying a constant speed of 500 RPM via the load machine. The tracking performance is shown in Fig. 4. During this test, the input constraints were circular with a radius of 8V (around double of what the machine would require to generate the reference currents). The voltage vector trajectory in the stationary $\alpha - \beta$ plane for the whole measurement is shown in Fig. 5. After that, to test the constraints fulfillment, the circular voltage constraints are set to a radius of 4V, where the same reference current profile have been applied (thus, the current tracking is hindered when higher voltages are required). As can be seen from Fig. 6 , the constraints were fulfilled accurately, and consequently the current flowing was limited.

To compare the performance of all of the mentioned controllers in this paper, two scenarios are considered as follows:

Scenario 1: The controllers have to maintain constant reference currents $(i_d^{ref} = 2A, i_q^{ref} = 4A)$, while the mechanical speed is stepped up from 400 RPM to 700 RPM, and then stepped down to 200 RPM. The results of
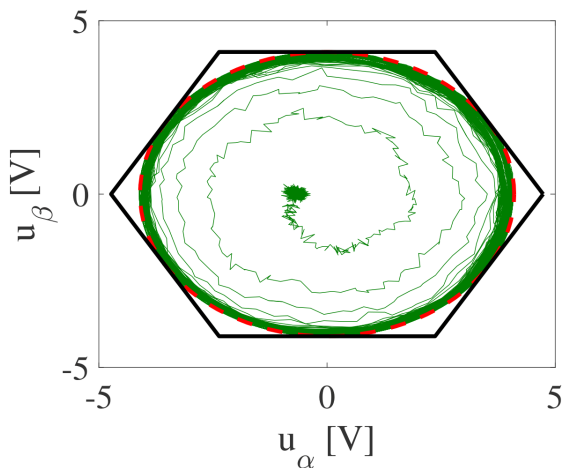
Fig. 6. Voltage trajectory when the VV magnitude was constrained to 4V

the FOC-PI controller, the DB-MPCC, the DB-MPCC-I, and the proposed CCS-MPCC are shown in Fig. 7, Fig. 8, Fig. 9, Fig. 10, respectively.

From the results of this test scenario, the following can be observed:

- The current tracking capability of the FOC-PI controller got highly affected when the speed of the load machine was changed at $t = 10$s and $t = 25$s.
- The DB-MPCC suffers from clear offsets (mainly because of parameters mismatch and inverter non-linearity), and hence, is not able to accurately track the desired references. Furthermore, with different load variations, different amplitude of offsets can be observed.
- By adding an integrator to the feedback loop, the DB-MPCC-I achieved a zero offset tracking of the reference currents, however, it gets affected by the variation of the load speed similarly as with FOC-PI due to the accumelation of the error.
- The proposed CCS-MPCC is very robust against load variation, as shown in Fig. 10.

Scenario 2: In this test, the mechanical speed was fixed to 500 RPM via the load machine, and the 4 controllers of the main machine were given a constant $i_d^{ref} = 2$A. A step change of the torque producing current i_q^{ref} from 3A to 7A has been applied. The results of this test for the four controllers are depicted in Fig. 11, and the currents are filtered by taking the mean of each 50 samples and are shown in Fig. 12. From this test, it is observed that the proposed CCS-MPCC has the fastest dynamical response, and it is the only controller which does not have cross coupling effects. It worth mentioning that, even though the DB-MPCC-I achieves no offset at steady-state, but the ripple is higher than the FOC-PI and CCS-MPCC.

9. CONCLUSION

In this paper, a CCS-MPCC including embedded integrators by using the input increments as decision variables to control synchronous machines is proposed. The single-shooting optimization problem is solved online for a horizon of two, while accounting for the nonlinear constraints
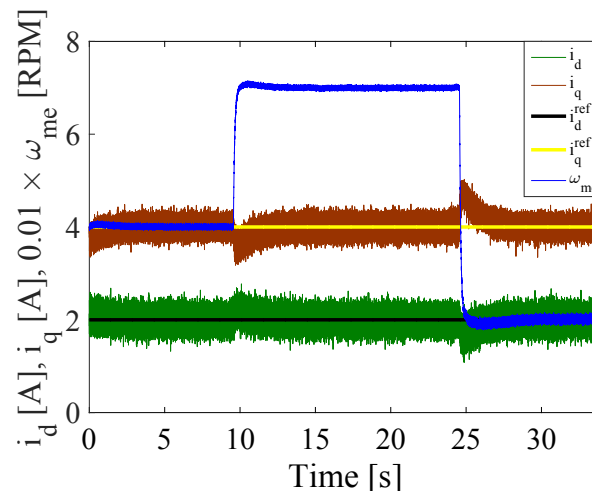
Fig. 7. Speed variation test of the FOC-PI controller
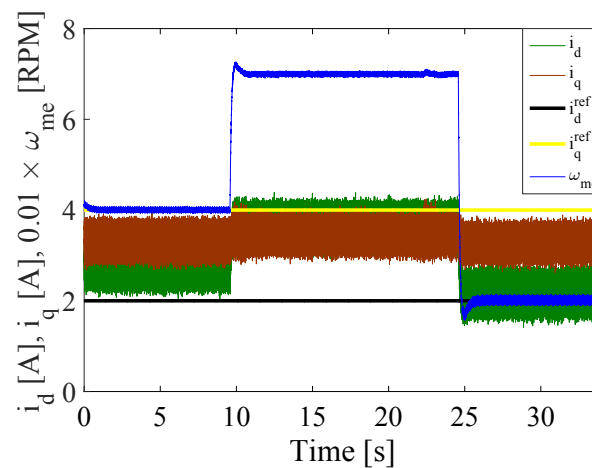
Fig. 8. Speed variation test of the DB-MPCC controller
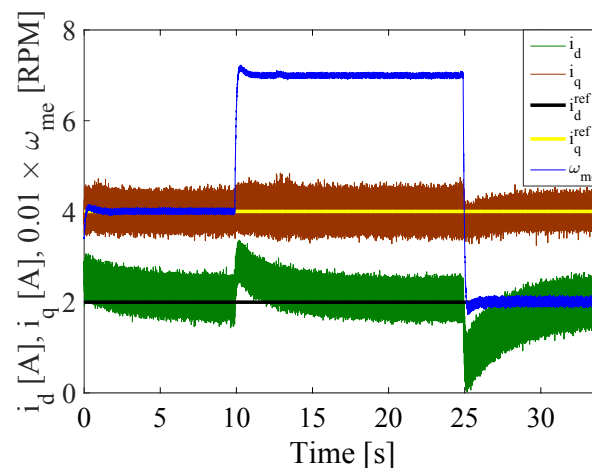
Fig. 9. Speed variation test of the DB-MPCC-I controller

using a slack formulation of the Primal-Dual Interior-Point method. By experimental results, the proposed controller has outperformed the state of the art FOC-PI, DB-MPCC, and DB-MPCC-I in transients and steady-state. Furthermore, it has shown the best and robust performance against load variations. In future work, it is planned to extend this formulation to longer horizon as well as the
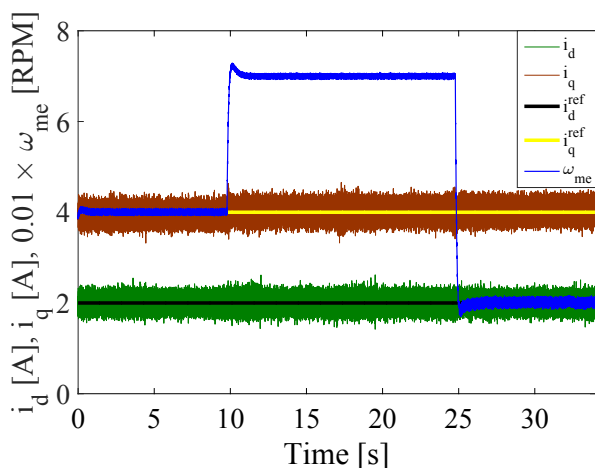
Fig. 10. Speed variation test of the proposed CCS-MPCC controller
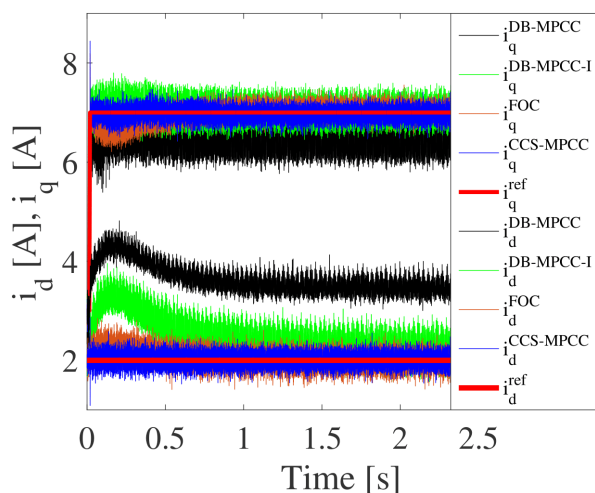
Fig. 11. Performance of all controllers under a step change of the torque producing current from 3A to 7A at a fixed speed of 500 RPM and a fixed $i_d^{ref} = 2A$
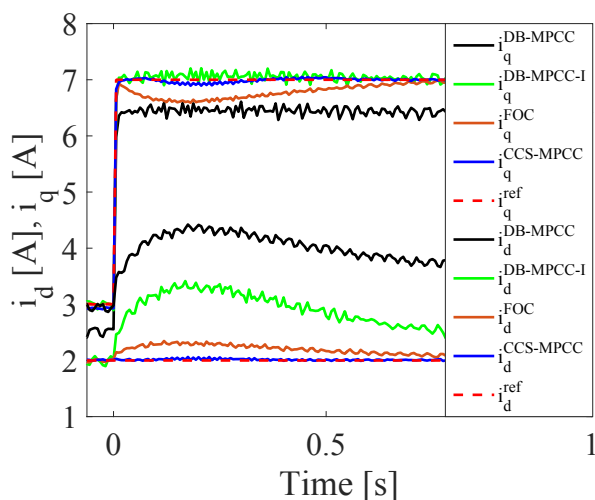
Fig. 12. Filtered averaged currents around the transient instant of the i_q step change test illustrated in *Scenario 2*

dimensions of the optimization problem to get the most of the MPC potential in electrical drives applications.

REFERENCES

Diehl, M. (2016). Interior point methods. In *Lecture Notes on Numerical Optimization*. URL https://www.syscop.de/teaching/ws2015/numopt.

Hackl, C.M. (2017). Non-identifier based adaptive control with internal model. In *Non-identifier Based Adaptive Control in Mechatronics*, 287–317. Springer International Publishing. doi:10.1007/978-3-319-55036-7_10. URL https://doi.org/10.1007\%2F978-3-319-55036-7_10.

Hammoud, I., Hentzelt, S., Oehlschlaegel, T., and Kennel, R. (2019). Computationally efficient finite-set model predictive current control of interior permanent magnet synchronous motors with model-based online inductance estimation. In *IEEE Conference on Power Electronics and Renewable Energy (CPERE)*, 1–6.

Hanke, S., Wallscheid, O., and Böcker, J. (2019). Continuous-control-set model predictive control with integrated modulator in permanent magnet synchronous motor applications. In *2019 IEEE International Electric Machines Drives Conference (IEMDC)*, 2210–2216. doi:10.1109/IEMDC.2019.8785122.

Huynh, T.A. and Hsieh, M.F. (2018). Performance analysis of permanent magnet motors for electric vehicles (ev) traction considering driving cycles. *Energies*, 11(6). doi:10.3390/en11061385. URL https://www.mdpi.com/1996-1073/11/6/1385.

Kennel, R., Linder, A., and Linke, M. (2001). Generalized predictive control (gpc)-ready for use in drive applications? In *2001 IEEE 32nd Annual Power Electronics Specialists Conference (IEEE Cat. No.01CH37230)*, volume 4, 1839–1844 vol. 4. doi:10.1109/PESC.2001.954389.

Lascu, C., Boldea, I., and Blaabjerg, F. (2004). Variable-structure direct torque control - a class of fast and robust controllers for induction machine drives. *IEEE Transactions on Industrial Electronics*, 51(4), 785–792. doi:10.1109/TIE.2004.831724.

Schröder, D. (2009). *Elektrische Antriebe - Regelung von Antriebssystemen*. Springer Berlin Heidelberg. doi:10.1007/978-3-540-89613-5. URL https://doi.org/10.1007\%2F978-3-662-06948-6_7.

Sharma, R. (2019). δu formulation for integral action. In *Lecture notes for the course IIA 4117: Model Predictive Control*, 104–105. URL https://web01.usn.no/~roshans/mpc/downloads/lecture_notes_MPC.pdf.

Wang, Y. and Boyd, S. (2010). Fast model predictive control using online optimization. *IEEE Transactions on Control Systems Technology*, 18(2), 267–278. doi:10.1109/TCST.2009.2017934.

Wiedemann, S. and Kennel, R.M. (2018). Accurate self-identification of inverter nonlinear effects in ac drives. In *PCIM Europe 2018; International Exhibition and Conference for Power Electronics, Intelligent Motion, Renewable Energy and Energy Management*, 1–70.

Young, H.A., Perez, M.A., and Rodriguez, J. (2016). Analysis of finite-control-set model predictive current control with model parameter mismatch in a three-phase inverter. *IEEE Transactions on Industrial Electronics*, 63(5), 3100–3107. doi:10.1109/TIE.2016.2515072.